Journal of Biomechanical Science and Engineering

Vol. 6, No. 2, 2011

Computational Fluid Dynamics of Blood Flow in an Extracorporeal Blood Circuit for the Analysis of Thrombogenic Hemodynamic Factors*

Masanori NAKAMURA**, Haruka TAKIMOTO*** and Shigeo WADA***

**Center for Advanced Medical Engineering and Informatics, Osaka University, Toyonaka, Osaka, Japan

E-mail: masanori@me.es.osaka-u.ac.jp

***Graduate School of Engineering Science, Osaka University, Toyonaka, Osaka, Japan

Abstract

Blood flow in a filter for an extracorporeal blood circuit was analyzed numerically to assess fluid mechanical quantities related to thrombogenesis. Results showed stagnant flow regions, in particular at the downstream side of the ceiling of a filter. A particle tracking along with an evaluation of a shear stress exerted on a particle demonstrated that a particle experiences a large shear stress when passing through a pore of the filter. These results suggest that a platelet would be activated when it goes though the pore and could then aggregate with other activated platelets to develop into a thrombus beneath the ceiling of a filter. Based on this hypothesis, the filter design was modified by making a protrusion on the downstream side of the filter. The protrusion design was varied in two ways in shape (sharp, blunt) and three ways in height (¼, ⅓, ½ of the height of the original filter). The simulation results showed a positive contribution of the protrusion to a decrease in the stagnant flow region on the downstream side of the filter ceiling. A comparison of the stagnant volume for models between a model with blunt protrusion and the one with sharp protrusion revealed that the blunt protrusion decreased the stagnant region more than that for models with a shape one. The protrusion also contributed to decreasing the shear stress at pores of the filter. This effect was more pronounced with an increase in the height of the protrusion. These results address benefits of the protrusion in the anti-thrombogenic design of a filter for an extracorporeal blood circuit.

Key words: Thrombus, Shear Stress, Stagnation, Extracorporeal Blood Circuit, Computational Fluid Dynamics

1. Introduction

Extracorporeal filters are used to remove gas bubbles, microthromboemboli, and aggregates composed of platelets, red blood cells, and other debris from blood in extracorporeal blood circulation before the blood is returned to the circulation of a patient. In clinical practice, these filters are often used for more than 3 h, long enough to trigger leukocyte activation and inflammatory mediators, including platelet-activating factors. Indeed, it is sometimes reported that the filters get clogged by thrombi, which form on the filter surface while in use.

*Received 12 Jan., 2011 (No. 11-0026)
[DOI: 10.1299/jbse.6.89]

Copyright © 2011 by JSME

Anticoagulant drugs are used to inhibit blood coagulation during such extracorporeal blood circulation. However, special care must be taken in the selection and usage of appropriate anticoagulants because some anticoagulants can induce allergic responses[1],[2]. Additionally, the use of anticoagulants should be avoided in patients with known bleeding disorders, elderly patients, and pregnant women[3].

From an engineering standpoint, coating techniques using hydrophilic polymers and heparin have been developed to improve hemocompatibility of the artificial surfaces of extracorporeal circuits[4]. Studies have demonstrated that biocompatible coatings can be quite effective in enhancing the antithrombogenic nature of artificial hearts[5] and other medical devices[6]-[8]. Nevertheless, coatings have basically been developed for the long-term use of medical devices, and are costly. In contrast, extracorporeal filters are disposable, and thus such coatings are problematic in terms of cost.

A thrombus is a blood clot. Although the complete process of thrombus formation remains unknown, it is accepted that it begins with activation of platelets under high wall-shear stresses[9]-[11]. It is also known that blood tends to form clots in stagnant flow[12]. Many experimental and clinical data indicate an association between hemodynamics and the risk of thrombus formation[13]. Conversely, inhibition of thrombus formation may be achieved by regulating the hemodynamics of blood passing through extracorporeal filters.

In the present study, we investigated hemodynamic factors that promote thrombus formation on an extracorporeal filter of a basic design. In particular, we evaluated fluid shear stresses, which are thought to activate platelets, and the size of stagnation within the filter, where activated platelets can aggregate to develop a thrombus. Filter designs were changed based on the results obtained with the filter of the basic design. On the basis of our results, we discuss a filter design that offers improved thrombogenic performance.

2. Methods

2.1 Geometry of extracorporeal filters

The geometry of the extracorporeal filter analyzed in this study is illustrated in Figure 1. The filter was a circular truncated cone with a height (L) of 25.0 mm, a ceiling diameter of 9.7 mm, and a base diameter of 20.0 mm. The filter had pores in its ceiling and side walls. In the ceiling, three circular ring arc pores with a width of 2.0 mm and a height of 0.25 mm formed a pitch circle with a radius of 3.0 mm. The pores in the side wall were rectangular with a width of 2.6 to 4.2 mm and a height of 0.34 mm. They were arranged by height in 26 rows and equiangularly in 12 columns. To further explain, a Cartesian coordinate system (x_1, x_2, x_3) was defined at the origin (O), placed at the center of the filter ceiling such that the x_3 axis was in the center line of the filter. The filter had three rotational symmetries about the x_3 axis. The side wall was angled at 7° to the x_3 axis. A filter of this geometry is said to have a basic design.

In addition to the filter of basic design, filters with protrusions in the ceiling were also investigated. Unless otherwise noted, the geometry of the filters, with the exception of changed portion(s), was the same as that of the basic design. Two protrusion types were prepared: blunt and sharp. A filter with a blunt protrusion was called “Case A,” while the one with a sharp protrusion was called “Case B.” Although the protrusions had parabolic shapes in both cases, the difference was in their widths. In Case A, the base diameter of the protrusion was the same as that of the filter ceiling, whereas it was half of that of the ceiling of Case B. As depicted in Figure 2, we prepared filters with various protrusion heights (¼, ⅓, ½ of the filter’s height, L). Filters with these protrusions were named according to the protrusion shape and height. For instance, a filter with a blunt protrusion and height of ¼ L was called “Case A-L/4.”

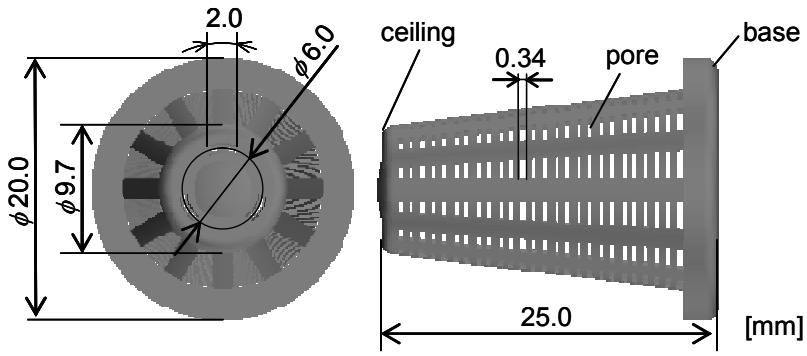


Figure 1. Geometry of the filter of basic design

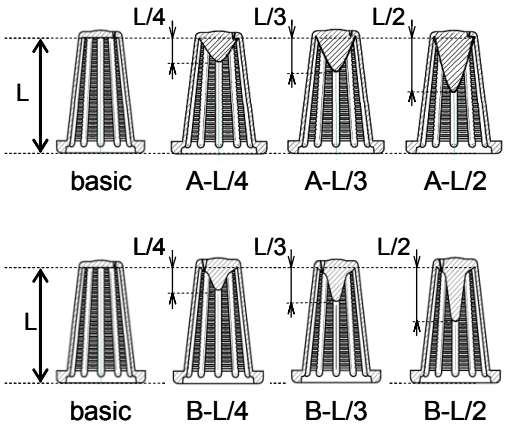


Figure 2. Geometry of filters with protrusions. Case A filters had a blunt protrusion at the ceiling, while Case B filters had a sharp protrusion.

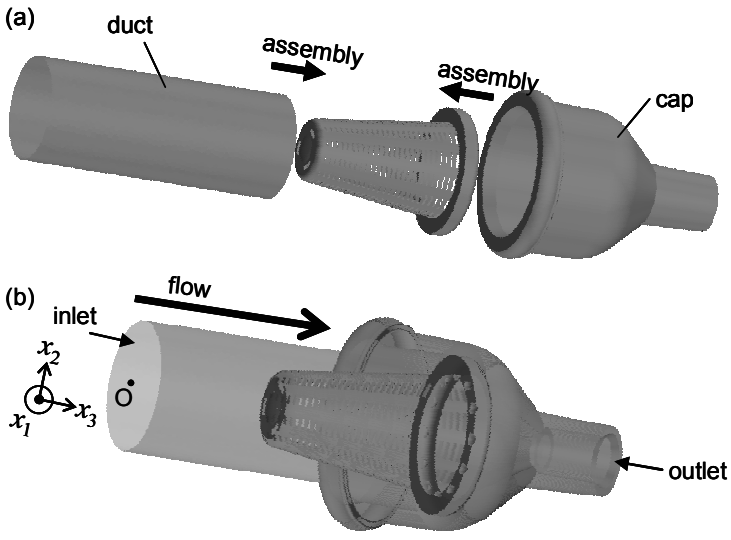


Figure 3. The filter was sandwiched by a circular duct and a cap for use. (a) Before assembly. (b) After assembly.

2.2 Blood flow analysis

Computational meshes were created for a region of blood flow. Taking clinical use into account, we assembled the filter by sandwiching it between a circular duct with a diameter of 16 mm and length of 42 mm on the upstream side (ceiling side) and a cap with the outlet conduit on the downstream side (Fig. 3). Computational meshes were then created for the inside of this filter set using the commercial software "STAR-CCM+" (CD-adapco, Japan). A prism layer mesh was used in the vicinity of the wall, whereas polyhedral meshes were adopted for the rest of the flow region. Meshing parameters were 1 mm for a base mesh size, 10% of the base mesh size for a relative size of prism layer thickness, 10% of the base mesh size for a surface minimum size, and 10% for a wrapper scale factor. These parameters resulted in 10,050,540 nodes and 1,879,294 elements for the filter of basic design. The base mesh size and wrapper scale factor are both parameters that determine the size of surface meshes to create polyhedral meshes. For more details, see the manual of STAR-CCM+[14].

Extracorporeal blood circulation is usually carried out at a constant flow rate of 200 mL/min (3.33×10^{-6} m^3/s). Thus, a steady flow was assumed in the blood flow analysis. Because of the presence of hemocytes, such as erythrocytes and leukocytes, blood is essentially a non-Newtonian fluid. However, because the non-Newtonian nature of blood has secondary effects on blood flow compared with the geometry of a flow region[15], blood was treated as an incompressible Newtonian fluid with a density (ρ) of 1050 kg/m^3 Pa and a viscosity (μ) of 0.0035 Pa·s. Furthermore, flow was assumed to be laminar because the Reynolds number assessed at the inlet of a circular duct was approximately 80. Flow simulations were performed by solving the Navier-Stokes equations along with the equation of continuity, given by

$$u_j \frac{\partial u_i}{\partial x_j} = -\frac{1}{\rho}\frac{\partial p}{\partial x_i} + \frac{\mu}{\rho}\frac{\partial^2 u_i}{\partial x_j \partial x_j} \tag{1}$$

$$\frac{\partial u_i}{\partial x_i} = 0 \tag{2}$$

where u_i is the component i of a velocity vector **u** (u_1, u_2, u_3), and p is pressure. The Einstein summation convention was used in writing the equations. The equations were solved in STAR-CCM+, which adopts a finite volume method for discretization. Convergence of the numerical solution was assessed based on the maximum tolerance of pressure of 1.0×10^{-4}. Boundary conditions were defined by taking into account the situation in which the filter is in clinical use (*i.e.,* flow at 200 mL/min). The boundary conditions applied were a spatially uniform velocity of 0.0166 m/s at the inlet, zero pressure at the outlet, and zero velocity with a nonslip condition on the wall.

When provided a velocity field, mass-less particles are traced using the Euler method. For this analysis, fluidic quantities of velocity and pressure obtained with prism and polyhedral meshes are interpolated to a new mesh field consisting of tetrahedral elements. A shear stress that exerts on a particle while flowing is evaluated with the Tresca stress criterion. Fluid mechanically, the stress tensor σ_{ij} at **x** (x_1, x_2, x_3) is given by

$$\sigma_{ij} = \begin{cases} \mu\left(\dfrac{du_i}{dx_j} + \dfrac{du_j}{dx_i}\right) & (i \neq j) \\ 2\mu\dfrac{du_i}{dx_j} - p & (i = j) \end{cases} \tag{3}$$

where u_i is the component i of the fluid vector, and p is static pressure. The stress tensor was

practically calculated by using shape functions of first-order tetrahedral elements and interpolating a fluid velocity field within an element where a particle of interest is present. The maximum shear stress τ_{max} is half of the maximum of the difference between any two eigenvalues σ_1, σ_2, σ_3 of the stress tensor σ_{ij}. Mathematically, this is expressed as

$$\tau_{\max} = \frac{\max\left|\sigma_i - \sigma_j\right|}{2} \tag{4}$$

and the Tresca stress σ_t is thereby calculated from

$$\sigma_t = 2\tau_{\max} \tag{5}.$$

3. Results

3.1 Filter of basic design

Trajectories of particles that passed through the filter of basic design are plotted in Figure 4. For clear visualization, the duct and the cap were removed. Here, the trajectories are color-coded according to the magnitude of fluid velocity (see the color bar on the right). As illustrated, particles that flowed in went almost straight ahead to the filter. While some of the particles flowed inside the filter by passing through pores in the ceiling of the filter, many went around the ceiling and passed through the pores in the side wall. The flow velocities were low during flow, but instantaneously increased when the particles passed through the filter pores, although that is not clear from this figure.

A contour plot of the velocity magnitude in the x_1–x_3 plane is provided in Figure 5. The magnitude of fluid velocity is scaled according to the color bar on the right. As illustrated, the filter of basic design primarily had three flow regions of low velocity or stagnation. The first was found at the upstream side of the ceiling, on which blood strikes (Zone A). The second was located at the downstream side of the ceiling (Zone B). The third was a junction between the filter and the cap (Zone C). Of the three, the second flow region distal to the ceiling was the largest.

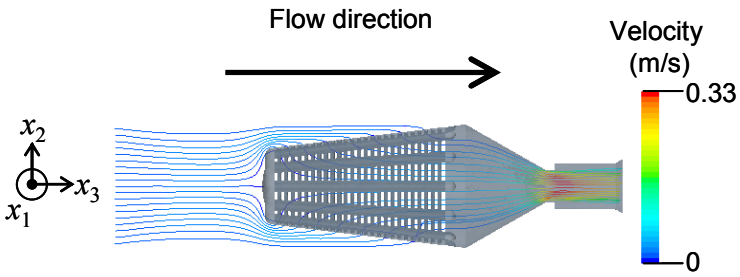


Figure 4. Particle traces for the filter of basic design

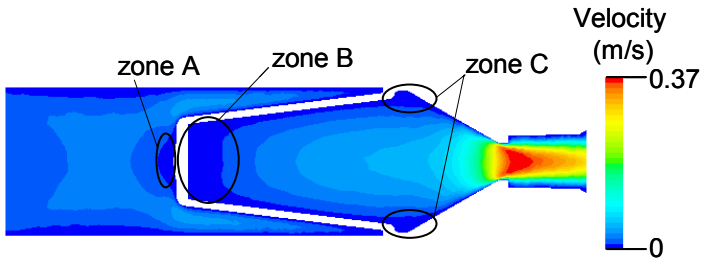


Figure 5. Contour plot of the velocity for the filter of basic design

Figure 6 (a) illustrates the trajectory of a particle that passed through a stagnant flow region beneath the ceiling (Zone B in Fig. 5). This particle was introduced at the center of the duct, flowed straight ahead to the ceiling, and changed directions to the side wall before the ceiling. It then passed through pores in the side wall to enter the stagnant flow region. The shear stress, or Tresca stress, that this particle experienced while flowing is plotted in Figure 6 (b). Here, the abscissa indicates the travel distance from the inlet, expressed in the x_3 coordinate. The red line and the black line represent the velocity magnitude and the shear stress, respectively. As illustrated, while the shear stress was approximately 0.01 Pa near the

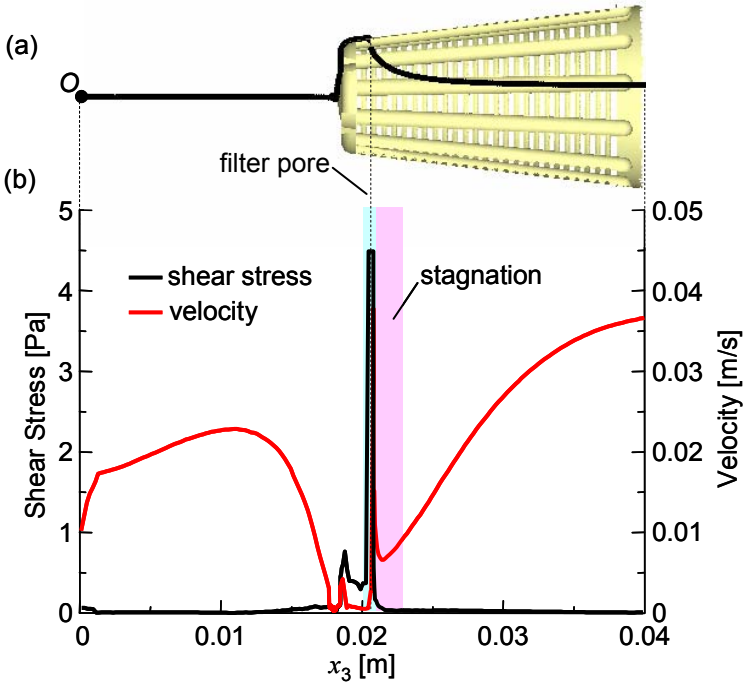


Figure 6. (a) Trace of a particle that enters a stagnation region under the ceiling of the filter. (b) Change in the shear stress and velocity of a particle along its flow trace in the basic design.

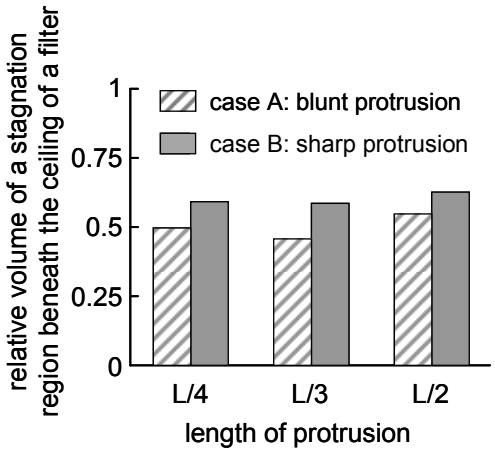


Figure 7. Comparison of the stagnation flow volume beneath the filter ceiling

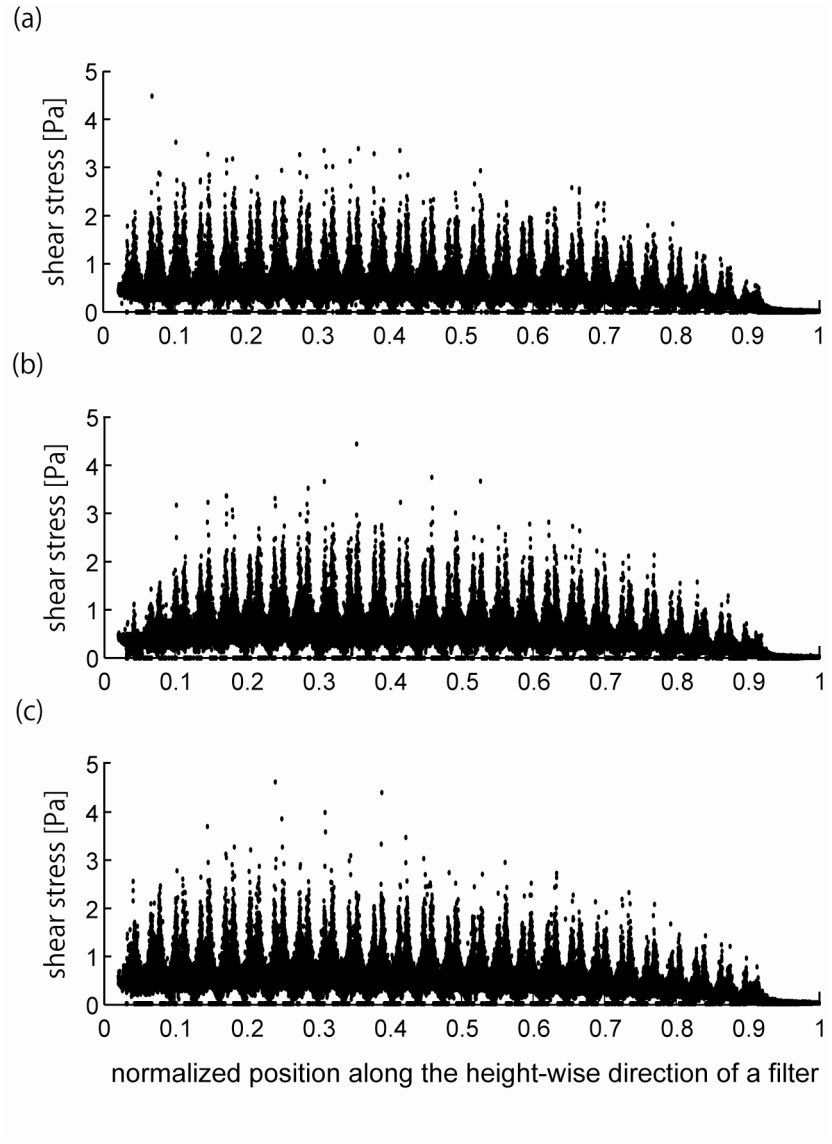


Figure 8. Plots of shear stress around filter pores for (a) basic design, (b) Case A-L/3, and (c) Case B-L/3

inlet, it increased markedly at approximately x_3 = 0.02 when the particle was passing through the filter pore. The flow velocity was found to decrease before and after the abrupt increase in shear stress at the filter pore.

3.2 Filters with protrusions in the ceiling

Flow patterns in the filters with protrusions, Cases A and B, were similar to the one observed in the filter of basic design. However, in both Cases A and B, particles that entered the filter by passing through side wall pores near the ceiling tended to flow smoothly to the outlet without staying in the flow region under the ceiling.

3.3 Comparison of flows in filters of various designs

The volume of the stagnant flow region under the ceiling was quantified by defining it as having a flow velocity $|\mathbf{u}|$ of <0.0066 m/s. Figure 7 presents the relative volume of the stagnant flow region when the volume of each filter design was compared with that of the filter of basic design. Compared with the basic design, the volume of the stagnant flow

region was decreased significantly by making a protrusion at the ceiling. The figure also shows a larger decrease in the stagnant flow volume for filters with blunt protrusions (Case A) when the protrusion had the same height. In contrast, as long as the shape type of the protrusion was the same, there was no significant variation in volume of the stagnant flow region even when the protrusion height was increased.

A spatial distribution of the shear stresses at nodal points on and near the side wall is plotted in Figure 8. Figures 8 (a), (b), and (c) contain the data for the basic design, Case A-L/3 and Case B-L/3, respectively. The abscissa Z shows a normalized coordinate of x_3 equal to 0 at the ceiling and 1 at the downstream end of the filter. Intermittently prominent data points in this figure represent nodal points at the filter pores. A comparison of Figures 8 (a) and (b) demonstrates some decreases in the shear stress near the filter ceiling (Z = 0–0.1) for Case A-L/3 (Fig. 8 (b)). Note that in Case A a longer protrusion contributed to reducing the shear stresses in a more downstream region. In contrast, the shear stresses for case B-L/3 (Fig. 8 (c)) were almost comparable to the ones observed for the basic design (Fig. 8 (a)). The shear stresses at the filter cores nearest to the filter ceiling decreased slightly when the protrusion was further longer (Case B-L/2).

By tracing approximately 200 particles that passed through filter cores where the shear stress was high, we found that more than 60 percents of particles outflowed without entering the stagnation flow region in all cases having the protrusion except Case B-L/4. In contrast, in the basic filter and Case B-L/4, only 30 percents of particles could avoid the stagnation flow region. On comparing the time required for particle that entered the stagnation flow region to exit, we found that the time was the shortest for the filter of basic design, but nearly the same for the filters of other designs.

4. Discussion

The present study analyzed the hemodynamics of blood passing through extracorporeal filters of basic and revised designs. Similar to this study, many studies in the past have attempted to investigate blood flow in medical devices to assess their thrombogenic nature. In most of these studies, flow patterns and shear stresses were prominent interests because they are both related to thrombus formation, but they were discussed separately[e.g., (16)-(19)]. Although the detailed mechanisms remain unclear, thrombus formation is achieved via the activation of platelets and their subsequent aggregation with other platelets and/or fibrin (and other components of blood). To date, it is accepted that the former is induced by exposure to high shear stress, while the latter is enhanced in a stagnant flow region (a low shear stress region)[(13)]. In view of such a biomechanical mechanism of thrombus formation, evaluation of shear stress only gives information on the degree of platelet activation, while evaluation of velocity provides the location of stagnant flow. Thus, separate discussions on these topics do not provide insight into whether activated platelets really enter stagnant flow regions to form thrombi. For better assessment of thrombogenic behavior, it is necessary to link information on velocity with that on shear stress. In the following discussion, we explore the thrombogenic nature of extracorporeal filters by regarding platelets as particles and analyzing their trajectories in combination with the shear stresses that they experience while flowing.

It is known from clinical experience that a thrombus is sometimes formed on the downstream side of the ceiling of filters of basic design. As shown in Figures 4 and 6, particles are exposed to high shear stresses when they pass through filter pores. If we regard platelets as particles, we suggest that platelet activation is induced at such filter pores. Furthermore, according to particle trajectories, after exposure to high shear stresses, the particles enter the stagnant flow region under the ceiling. This indicates that formation of a thrombus on the downstream side of the ceiling results from platelets that have been activated at filter pores and then bind with other platelets or other blood components in the

stagnant flow. Conversely, to inhibit thrombus formation on the downstream side of the ceiling, the filter design should be changed such that shear stresses at filter pores are decreased and flow under the ceiling is smoothened to reduce or avoid stagnation under the ceiling.

A protrusion was made on the downstream side of the ceiling to reduce the volume of stagnant flow. This protrusion physically occupied the flow region under the ceiling, decreasing the stagnant flow volume (Fig. 7). As shown in Figure 7, if the protrusion had the same height, a larger decrease in stagnant flow volume was achieved for Case A, which had a blunt protrusion. This is simply attributable to the difference in the volume of the protrusion between Cases A and B, the former of which bulges more. In addition to physically occupying the space under the ceiling, as is clear from Fig. 8, the protrusion of Case A offered a flow resistance to blood that tried to enter the filter through the pores near the ceiling, while that of Case B did not so much. This suggests that the protrusion may have depressed the degree of platelet activation at the filter pores. In fact, when we traced a particle placed at the same initial position as the one in Figure 6 and calculated the shear stress along its path for the filter of Case A-L/3, we found that the shear stress exerted on the particle was 1.2 Pa at maximum. Moreover, the protrusion helped to redirect blood coming through the pores near the ceiling so that it flowed straight ahead to the outlet of the filter. That is, even if the platelets were activated at the filter pores, they exited the filter without staying in the stagnant flow. Based on these results, we suggest that it may be possible to enhance the antithrombogenic nature of an extracorporeal filter by adding a protrusion on the downstream side of the ceiling.

Although this paper presents the results for filters having a protrusion on the downstream side of the ceiling, we also investigated filters of other designs: specifically, filters with halved or doubled heights and those in which the side walls were inclined at 0° or 12° against the central axis (x_3 axis). Note that "stagnation" or other synonymous words in this paragraph refer to the one formed under the ceiling which was illustrated as zone B in Fig. 5. When the filter height was halved, the volume of stagnation under the ceiling decreased, but shear stresses at the filter pores increased to more than two-fold at maximum. In the filter with doubled height, the stagnant flow was increased, whereas shear stresses at filter pores were reduced. A change in the inclination angle of the side wall to 0° brought about a significant decrease in the stagnation volume under the ceiling. However, coincidentally, shear stresses at the filter pores near the ceiling increased five-fold compared with those for the filter of basic design. In contrast, when the side wall was angled at 12°, the stagnation region under the ceiling expanded, while shear stresses at pores near the filter ceiling became one-third of those in the filter of basic design. These results demonstrate that changes in the filter height and side wall angle improve one of the hemodynamic factors we have discussed so far, but cause others to deteriorate. Thus, these changes may not always improve the antithrombogenic nature of an extracorporeal filter.

The present study has some limitations. First, we evaluated shear stresses, which are instantly exerted on particles as an index of platelet activations. In addition to instantaneous shear stresses, some studies have assessed cumulative shear stresses[20]-[22]. In fact, it has been experimentally demonstrated that high shear alone is likely insufficient for the induction of platelet activation, and the platelet response to high shear depends on the duration of shear exposure[23] during which mechanical stimuli due to shear stresses acting on platelets are accumulated. One of the problems to model the cumulative shear-activation process of platelets is setting of the proper duration of shear exposure to calculate cumulative shear stress. Second, adhesiveness of platelets to walls was not considered in this study. As Tamagawa *et al.*[24] showed, the adhesiveness of platelets to a surface strongly affects thrombus development. Thus, the present analysis does not establish whether platelets that are activated at filter pores and aggregate in stagnant flow really develop into a

thrombus on the downstream side of the filter ceiling, as sometimes observed in clinical practice. If platelet adhesivity to a filter surface is quite strong, the presence of protrusion at the filter ceiling might cause a negative effect on anti-thrombogenic nature of the filter. In particular, an increased surface area with a higher protrusion would provide more chances to activated platelets to adhere to the surface. Hence, in such a case, we need to optimize the protrusion height to deal with the trade-off between reduction of the stagnation under the ceiling and an increase in chances of platelet adhesions to the surface. Notwithstanding these limitations, analysis of shear stresses in combination with particle trajectories will help provide biomechanical insight into the thrombogenic mechanisms of medical devices, although we did not take into account detailed biochemical cascades of thrombus formation, as Fogelson and Tania[25] did. In the future, we will carry out an *in vitro* experiment of thrombus formation to demonstrate the validity of the present simulation, and include the duration of shear exposure and adhesiveness of platelets in the analysis for a better assessment of the thrombogenic nature of extracorporeal filters.

5. Summary and Conclusions

Hemodynamic factors were analyzed numerically to investigate the thrombogenic effects of extracorporeal filters. The results for the filter of basic design indicated that platelets were exposed to high shear stresses while passing though the filter pores near the ceiling and then entered a stagnant flow region where they could bind with other platelets, form an aggregate, and develop into a thrombus. Thus, we hypothesized that thrombus inhibition on the downstream side of the ceiling could be achieved by breaking the stagnant flow and decreasing the shear stresses at the filter pores near the ceiling. Based on our results, the filter design was changed such that the downstream side of the ceiling protruded. The protrusion physically occupied the flow region under the ceiling where the flow was stagnant in the filter of basic design and reduced shear stresses at the pores near the ceiling. These results suggest that adding a protrusion to the downstream side of the ceiling can be effective in inhibiting thrombus formation on the downstream side of the ceiling and improves the antithrombogenic features of extracorporeal filters.

The present study demonstrated that hemodynamic factors associated with thrombus formation can be controlled by changing filter designs. This indicates that a change in geometric design can improve the antithrombogenic nature of medical devices without having to rely on anticoagulants or antithrombogenic materials. Because design changes are not costly, compared with the inclusion of additional processes such as coating, such approaches may be useful in inhibiting thrombus formation while saving production costs. In the future, we will focus on thrombi that form at other filter locations and improve filter designs so that they too have a more antithrombogenic nature.

Acknowledgements

The authors acknowledge receipt of a Grant-in-Aid for Young Scientists (A) 19680024 by Japan Society for the Promotion of Science (JSPS) and a Grant-in-Aid for Scientific Research (B) 22300155 by The Ministry of Education, Culture, Sports, Science and Technology (MEXT).

References

(1) Maruyama, H., Miyakawa, Y., Gejyo, F., Arakawa, M., Anaphylactoid reaction induced by nafamostat mesilate in a hemodialysis patient, *Nephron*, Vol. 74 (1996), pp. 468-469.

(2) Yamazato, M., Mano, R., Oshiro-Chinen, S., Tomiyama, N., Sakima, A., Ishida, A., Tana, T., Tozawa, M., Muratani, H., Iseki, K., Takishita, S,. Severe abdominal pain

associated with allergic reaction to nafamostat mesilate in a chronic hemodialysis patient, *Internal Medicine*, Vol. 41 (2002), pp. 864-866.

(3) Serebruany, M. V,. Malinin, A. I., Serebruany. V. L., Argatroban, a direct thrombin inhibitor for heparin-induced thrombocytopaenia: present and future perspectives, *Expert Opinion on Pharmacotherapy*, Vol. 7 (2006), pp. 81-89.

(4) Wendel, H. P., Ziemer, G., Coating-techniques to improve the hemocompatibility of artificial devices used for extracorporeal circulation, *European Journal of Cardio-thoracic Surgery*, Vol. 16 (1999), pp. 342-350.

(5) Koster, A., Loebe, M., Sodian, R., Potapov, E. V., Hansen, R., Müller, J., Mertzlufft, F., Crystal, G. J., Kuppe, H., Hetzer, R., Heparin antibodies and thromboembolism in heparin-coated and noncoated ventricular assist devices, *Journal of Thoracic and Cardiovascular Surgery*, Vol. 121 (2001), pp. 331-335.

(6) Devine, C., Hons, B., McCollum, C., Heparin-bonded Dacron of polytetrafluuroethylene for femoropopliteal bypass grafting: a multicenter trial, *Journal of Vascular Surgery*, Vol. 33 (2001), pp. 533-539.

(7) Saito, S., Westaby, S., Piggott, D., Katsumata, T., Dudnikov, S., Robson, D., Catarino, P., Nojiri, C., Reliable long-term non-pulsatile circulatory support without anticoagulation, *European Journal of Cardio-thoracic Surgery*, Vol. 19 (2001), pp. 678-683.

(8) Johnell, M., Elgue, G., Larsson, R., Larsson, A., Thelin, S., Siegbahn, A., Coagulation, fibrinolysis and cell activation in patients and shed mediastinal blood during coronary artery bypass grafting with a new heparin coated surface, *Journal of Thoracic and Cardiovascular Surgery*, Vol. 124 (2002), pp. 321-332.

(9) Ni, H., Freedman, J., Platelets in hemostasis and thrombosis: role of integrins and their ligands, *Transfusion and Apheresis Science*, Vol. 28 (2003), pp. 257-264.

(10) Andrews, R. K., Berndt, M. C., Platelet physiology and thrombosis, *Thrombosis Research*, Vol. 114 (2004), pp. 447-453.

(11) Tarnow, I., Kristensen, A., Olsen, L., Falk, T., Haubro, L., Pedersen, L., Pedersen, H., Dogs with heart diseases causing turbulent high-velocity blood flow have changes in platelet function and von Willebrand factor multimer distribution, *Journal Veterinary Internal Medicine*, Vol. 19 (2005), pp. 515–522.

(12) López, J. A., Chen, J., Pathophysiology of venous thrombosis, *Thrombosis Research*, Vol. 123, Suppl 4 (2009), pp. S30-34.

(13) Lowe, G. D., Virchow's triad revisited: abnormal flow, *Pathophysiology of Haemostasis and Thrombosis*, Vol. 33 (2003/2004), pp. 455-457.

(14) STAR-CCM+ User guide, Ver. 4.02.007, CD-Adapco, 2008, pp. 828-883.

(15) Ishikawa, T., Guimaraes, L. F. R., Oshima, S., Yamane, R., Effect of non- Newtonian property of blood on flow through stenosed tube, *Fluid Dynamics Research*, Vol. 22 (1998), pp. 251-264.

(16) Okamoto, E., Hashimoto, T., Inoue, T., Mitamura, Y., Blood compatible design of a pulsatile blood pump using computational fluid dynamics and computer-aided design and manufacturing technology, *Artificial Organs*, Vol. 27 (2003), pp. 61-67.

(17) Untaroiu, A., Throckmorton, A. L., Patel, S. M., Wood, H. G., Allaire, P. E., Olsen, D. B., Numerical and experimental analysis of an axial flow left ventricular assist device: the influence of the diffuser on overall pump performance, *Artificial Organs*, Vol. 29 (2005), pp. 581-591.

(18) Triep, M., Brücker, C., Kerkhoffs, W., Schumacher, O., Marseille, O., Investigation of the washout effect in a magnetically driven axial blood pump, *Artificial Organs*, Vol. 32 (2008), pp. 778-784.

(19) Izraelev, V., Weiss, W. J., Fritz, B., Newswanger, R. K., Paterson, E. G., Snyder, A., Medvitz, R. B., Cysyk, J., Pae, W. E., Hicks, D., Lukic, B., Rosenberg, G., A passively

suspended Tesla pump left ventricular assist device, *ASAIO Journal*, Vol. 55 (2009), pp. 556-561.

(20) Bluestein, D., Li, Y. M., Krukenkamp, I. B., Free emboli formation in the wake of bi-leaflet mechanical heart valves and the effects of implantation techniques, *Journal of Biomechanics*, Vol. 35 (2002), pp. 1533-1540.

(21) Dumont, K., Vierendeels, J., Kaminsky, R., Nooten, G. V., Verdonck, P., Bluestein, D., Comparison of the hemodynamic and thrombogenic performance of two bileaflet mechanical heart valves using a CFD/FSI model, *Journal of Biomechanical Engineering*, Vol. 129, (2007) pp. 558-565.

(22) Nobili, M., Sheriff, J., Morbiducci, U., Redaelli, A., Bluestein, D., Platelet activation due to hemodynamic shear stresses: damage accumulation model and comparison to in vitro measurements, *ASAIO Journal*, Vol. 54 (2008), pp. 64-72.

(23) Zhang, J., Bergeron, A. L., Yu, Q., Sun, C., McBride, L., Bray, P. F., Dong, J., Duration of exposure to high fluid shear stress is critical in shear-induced platelet activation-aggregation, *Thrombosis and Haemostasis*, Vol. 90 (2003), pp. 672–678.

(24) Tamagawa, M., Kaneda, H., Hiramoto, M., Nagahama, S., Simulation of thrombus formation in shear flows using Lattice Boltzmann Method, *Artificial Organs*, Vol. 33 (2009), pp. 604-610.

(25) Fogelson, A. L., Tania, N., Coagulation under flow: The Influence of flow-mediated tansport on the initiation and inhibition of coagulation, *Pathophysiology of Haemostasis and Thrombosis*, Vol. 34 (2005), pp. 91-108.